Desalination 558 (2023) 116613

Contents lists available at ScienceDirect

Desalination

journal homepage: www.elsevier.com/locate/desal

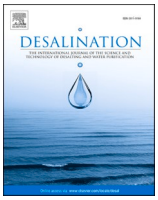

# Limiting current density as a selectivity factor in electrodialysis of multi-ionic mixtures

Pauline Zimmermann [a], Önder Tekinalp [b], Simon Birger Byremo Solberg [a], Øivind Wilhelmsen [c], Liyuan Deng [b], Odne Stokke Burheim [a,*]

[a] Department of Energy and Process Engineering, Norwegian University of Science and Technology (NTNU), NO-7491 Trondheim, Norway
[b] Department of Chemical Engineering, Norwegian University of Science and Technology (NTNU), NO-7491 Trondheim, Norway
[c] Department of Chemistry, Norwegian University of Science and Technology (NTNU), NO-7491 Trondheim, Norway

## HIGHLIGHTS

- A new method for determining limiting current in ED setup using Nernst equation
- The ion-specific limiting current promotes selectivity in multi-ionic mixtures.
- High $Cl/SO_4$ and $F/SO_4$ separation efficiencies in 1:1:100 mixtures of $Cl:F:SO_4$

## GRAPHICAL ABSTRACT

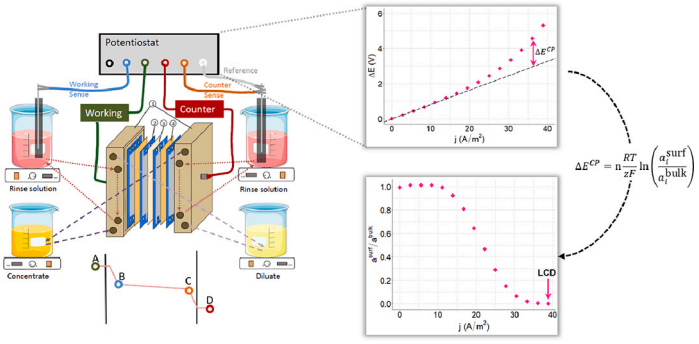


## ARTICLE INFO

*Keywords:*
Electrodialysis
Ion-exchange membranes
Monovalent selectivity
Limiting current density
Concentration polarization

## ABSTRACT

Electrodialysis is a promising technology to remove low concentrations of target ions from multi-ionic mixtures. While the synthesis of selective membranes is a prominent topic in research, few studies have been presented on selectivity-enhancing process design. This work investigates the limiting current density as a selectivity promoter in removing dilute target ions from a concentrated solution. Ambiguities and challenges in the prevailing definitions of the limiting current density are identified, and a new approach based on the Nernst equation is proposed, the boundary-layer method. Chloride and fluoride with starting concentrations of 10 mM were removed from 1 M sodium sulfate base electrolyte with varying current density levels around the limiting value. Removal rates, separation efficiencies, and energy consumption were compared. The separation efficiencies between chloride and sulfate and fluoride and sulfate had their highest values at 0.93 and 0.81, respectively, when operating at 130 $A/m^2$. We demonstrate that increasing the ion selectivity through the ion-specific limiting current density is possible and only requires standard current-voltage data. The experimental results suggest that process optimization is an essential supplement to membrane development to enhance the selective removal of target ions by electrodialysis.

* Corresponding author.
*E-mail address:* burheim@ntnu.no (O.S. Burheim).

https://doi.org/10.1016/j.desal.2023.116613
Received 16 January 2023; Received in revised form 23 March 2023; Accepted 7 April 2023
Available online 13 April 2023

## 1. Introduction

Membrane technology can play a crucial role in enabling sustainable industrial growth and transition due to its versatility, efficiency, and high selectivity, leading to more rational utilization of raw materials and recovery of by-products [1]. Electrodialysis (ED) is a promising technology within membrane processes for solution purification due to its high selectivity and capacity [2,3].

ED is an electro-membrane process where ions move in an electric field, passing anion- and cation-exchange membranes (AEMs and CEMs, respectively). A typical ED setup is illustrated in Fig. 1. Applying an electric potential across the cell establishes a charge imbalance in the stack, forcing cations towards the cathode, passing the CEM, and anions towards the anode, passing the AEM. Consequently, anions and cations are collected in every second compartment while every other compartment is desalinated [4]. The ions preferably transported across the membrane are called *counter-ions*, and the ions repelled by the membrane are called *co-ions*. Membranes can further be customized to feature selectivity of ions with the same charge; for example, monovalent-selective IEMs discriminate ions of higher valence [5].

Despite ED's benefits for solution purification and revalorization, large-scale industrial applications are limited [6]. The lack of upscaling can partially be attributed to membrane inefficiencies like low permeability and selectivity, low thermal and chemical resistance, and high cost. Alongside the development of superior membranes, process parameters like module design and hydrodynamics must be understood, and optimized [1]. Predominantly, process optimization addresses energy requirements and efficiency of ED setups. The transport rate of ions in ED increases with increasing current; however, the same is true for the loss of efficiency. Depending on the treatment goals, a practical minimum current is required to achieve a specific salt removal in a reasonable time. There is also a practical maximum current in ED, which is commonly called the limiting current.

The limiting current density (LCD) is dictated by membrane and solution properties, the ED stack design, and operational parameters such as flow velocity and temperature [7]. The applied current determines to a large extent the operational cell resistance and efficiency of the ED system [8]. It is, therefore, often recommended to operate ED at around 80 % of the LCD to limit power consumption and energy costs [9,10]. LCD determination methods have been developed for binary electrolytes [9,11–13] and multi-ionic mixtures considering complete desalination of the treated solutions [14–16]. Gorobchenko et al. developed a model that describes ion selectivity in a bi-layered monovalent selective CEM as a function of the current density. They suggest that changes in the kinetic control cause the dependence of the counter-ion selectivity on the current density according to three current regimes: (1) at low currents, the substrate membrane controls the ion selectivity, favoring the transport of multi-over monovalent ions, (2) with increasing current, the control passes to the selective layer, favoring the transport of mono-over multivalent ions, and (3) when the LCD of the mixture is reached, the membrane permselectivity becomes zero, and their diffusivity in the boundary layer controls the selectivity between counter-ions. In consequence, the dependence of the ion selectivity on the electric current density passes through a maximum [17]. Zabolotsky et al. describe a similar behavior of counter-ion selectivity in ternary mixtures as a function of current density, pointing out that a loss of permselectivity appears at the LCD due to the decrease of the boundary concentrations of the ions in the depleted diffusion layer to zero [18]. Geraldes and Afonso introduced the concept of a critical current density, $j_{i,crit}$, that defines the current density at which the concentration of a specific ion $i$ in a multi-ionic mixture approaches zero at the solution/membrane interface. They used the definition of the critical current density to determine the limiting transport number, $t^{m}_{i,lim}$, for which all counter-ion concentrations vanish simultaneously at the solution/membrane interface. The LCD for multi-ionic mixtures is estimated by adding the contributions of each ion based on its limiting transport number and concentration in the solution. For single salt and multi-ionic solutions, the developed model predicted LCDs that nearly matched the experimental data [15]. If the LCD of a multi-ionic mixture is the sum of each ion's contribution, the critical current density can be interpreted as ion-specific LCD, and operating ED at the specific LCD of a target ion could affect the separation efficiency between counter-ions.

In this work, we determine the ion-specific LCD in a membrane stack and investigate whether it can be used as a selectivity promoter. In particular, the removal of chloride and fluoride trace concentrations (10 mM) from a concentrated sulfate solution (1 M) is studied. In many industries, such as groundwater treatment, hydrometallurgy, and thermal power generation, an excess of chloride and fluoride accumulates in process solutions. Halides can be toxic for human and aquatic life and corrosive towards process equipment [19–21]. The respective electrolytes often also contain sulfate ions that can be revalorized as sulfuric acid or recirculated where it is needed in the process [22,23]. Various groups have studied selectivity between chloride and sulfate in ED, mostly investigating surface-modified or microstructure-tuned

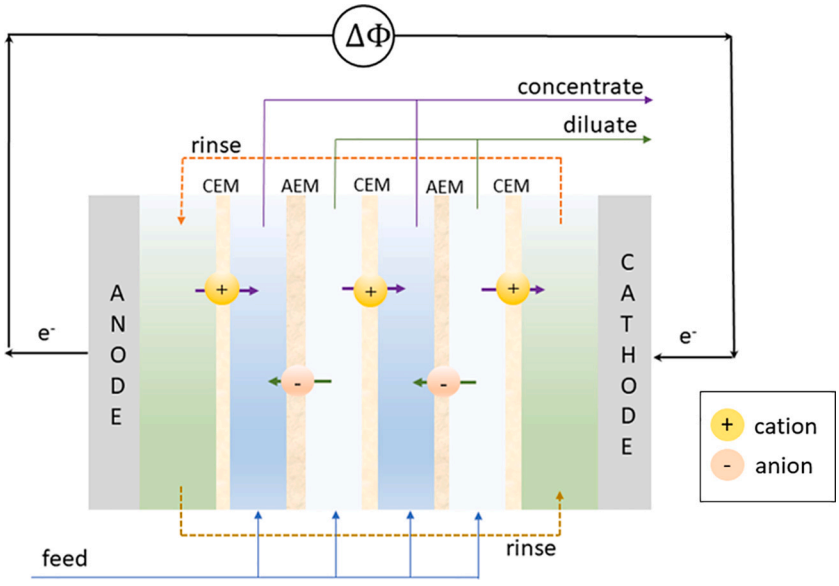


**Fig. 1.** Illustration of an ED stack. CEMs and AEMs are alternated between the electrodes. A rinse solution is circulated in the electrode compartments, where electrochemical reactions occur. Driven by the electric field, anions migrate towards the anode through the AEM, while cations migrate towards the cathode through the CEM. As a result, ions are concentrated in every second compartment while every other compartment is desalinated. The sketch illustrates a continuous ED operation, where the feed stream is divided into a concentrate and a diluate outlet stream; however, ED is often run in batch mode on the laboratory scale.

membranes. Equimolar concentrations of the two competing counter-ions ranging from 0.02 M to 0.5 M have been investigated [24–34]. Recently, a study has been performed on designing monovalent-selective AEM to remove chloride and fluoride from sulfate [35]. Kabay et al. investigated ED with selective removal of fluoride in the presence of chloride and sulfate by using an equimolar mixture with an initial concentration of 100 mg/L fluoride. The migration order of the ions was $Cl^- > F^- > SO_4^{2-}$ [36]. Arar et al. studied the separation of low fluoride concentrations (2 mg/L) from 1:25:25 mixtures with chloride and sulfate. ED was operated at 80 % of the LCD of the mixture. The removal rate of fluoride was higher (96 %) in the presence of both chloride and sulfate compared to binary mixtures of fluoride and chloride (63 % removal of F) and fluoride and sulfate (93 % removal of F), which was ascribed to the increased ionic strength of the solution. However, the same enhancing effect was observed for leakage of chloride and sulfate, which were removed by 98 % and 53 % in the ternary mixture, respectively [37].

By using the ion-specific LCD of chloride and fluoride, the ED unit is operated at the maximum transfer rate of the target ions, maximizing separation efficiency while limiting energy consumption. Our research identifies potential strategies for enhancing selectivity between like-charged ions through process optimization as a crucial completion to membrane development. A semi-empirical method to determine the LCD based on the Nernst equation is proposed, where the only experimental input needed is the recording of a current-voltage characteristic of the respective salts in the ED setup. The results are validated by performing desalination experiments at the apparent optimum current and lower and higher current values. The experiments are evaluated by tracking the removal rates of the anions, determining the separation efficiencies between chloride and sulfate as well as fluoride and sulfate, and comparing the energy consumption at the different current intensities. The LCD values are compared to those obtained by the Cowan-Brown and Isaacson-Sonin methods (CB and IS methods, respectively), two widely used techniques to determine the LCD.

## 2. Theory and principles

Due to the incomplete mixing of the solutions and typically high permselectivity of the IEMs, boundary layers form at the membrane surfaces. Within the boundary layers, concentration profiles arise. The concentration of counter-ions decreases from the bulk towards the membrane surface at the dilute side and increases towards the membrane surface at the concentrate side [38]. Fig. 2 shows such a concentration profile for chloride and sulfate, including bulk solutions, boundary layers, and an AEM. IUPAC recommends the term concentration polarization (CP) for such concentration profiles [39]. Due to CP, ion diffusion in the boundary layer occurs in the same direction of migration for counter-ions and in the opposite direction for co-ions to satisfy the local electroneutrality criterion. A lowered concentration of ions in the boundary layer increases the ohmic resistance and the energy input requirement to drive the ion transport [40,41]. The degree of CP increases as the electrodialytic current density increases due to the depletion of ions at the membrane/solution interface and the formation of steeper concentration profiles. When the concentration of counter-ions approaches zero at the membrane surface facing the dilute side, the LCD is reached, as shown for chloride in Fig. 2. Theoretically, no further increase in the rate of ion permeation can occur with an additional increment of current density [42].

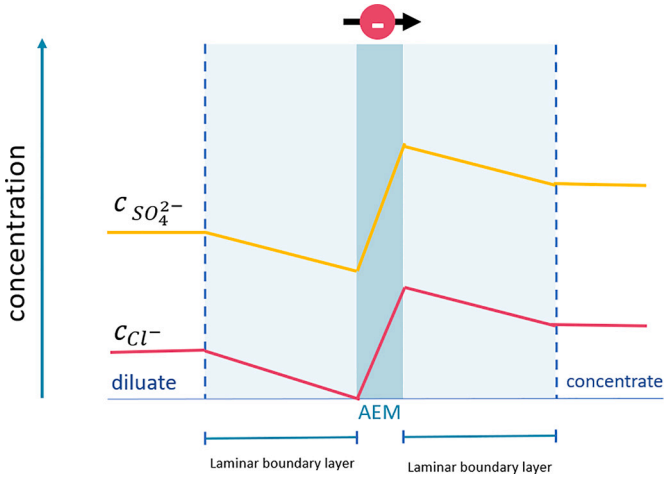


**Fig. 2.** Schematized concentration profiles of the two competing counter ions chloride and sulfate through an AEM and the adjacent diffusion boundary layers. Due to the lower concentration of chloride, it depletes at the membrane surface under lower applied currents than sulfate.

The limiting current is a concept used in a variety of electrochemical systems that describes a saturation of the current in a system. The charge transfer limitation is typically caused by insufficient diffusion rates of the reactants compared to the availability of electrons. It is, therefore, also called diffusion-limited current density [43]. In ED setups, there is no actual saturation of the current density. Instead, an increase of potential drop towards infinity can be observed when increasing the current from the ohmic regime to over-limiting values [44]. Three main mechanisms are found to be responsible for continued charge transfer at over-limiting current densities: (1) current-induced convection, (2) water splitting, and (3) co-ion leakage and current-induced membrane disintegration. For further insight into mass and charge transfer at over-limiting current, we refer to [45,46].

The deviation from the merely diffusion-controlled behavior leads to ambiguities in identifying the LCD in ED. Isaacson and Sonin state that even though there is no such value that represents an absolute physical upper bound to the current density, there is a practical upper bound for current density in ED desalination to avoid water dissociation, pH changes, and a drop in current efficiency (i.e., the amount of work input that results in charge transfer by ions through the membranes) [47]. According to Cowan and Brown, the LCD represents the first value where the current is diffusion limited [48]. In contrast, Nikonenko et al. describe the LCD as the current density at which the counter-ion concentration at the membrane surface becomes negligible compared to the counter-ion bulk concentration [45]. As a consequence of the different definitions of LCD, many empirical, semi-empirical, and theoretical approaches exist to determine LCD. There are several recent reviews of LCD determination methods [2,44,49], giving a comprehensive overview starting from the first advance made by Peers in 1958 [14] and ending with the introduction of a semi-empirical approach in 2019 by La Cerva et al. [44]. Purely empirical correlations for the LCD often predict the current saturation and therefore fail to describe the ED system adequately [44]. Despite a wide range of theoretical models to predict the LCD, in practical applications, it is generally experimentally determined [38]. The IS and CB techniques are two commonly used graphical methods to determine the LCD that require only the recording of current-voltage curves for the system of interest. The straight line indicating the ohmic region in the current-voltage curve is extrapolated using the IS method. A tangent is drawn past the turning point where the potential rises towards infinity. The LCD is identified as the intersection between those two lines. The apparent resistance, $\Delta E/j$, is plotted against the inverse current density using the CB method. The LCD is defined as the intersection between the trend line with a positive slope and that with a negative slope. Both of these methods use the LCD definition of the first diffusion-limited value. For complete desalination of the feed solution, going beyond that value often requires a drastic voltage increase that is not justified by a corresponding increase in ion removal/recovery. However, when removing target ions from a base electrolyte, the voltage increase after depletion of the target ions will be reasonable since the base electrolyte maintains enough ionic strength for charge transfer. Therefore, when using LCD as a tool for the selective

removal of counter-ions, it can be profitable to adopt the LCD definition of negligible counter-ion concentration at the membrane surface.

Ion depletion in the boundary layer is coupled with increasing cell resistance. The total cell potential across an ED cell is

$$\Delta E^{\text{cell}} = \Delta E^{OCV} + rj + |\Delta E^{CP}| \quad (1)$$

where $\Delta E^{OCV}$ (V) is the open circuit voltage, $r$ ($\Omega m^2$) is the ohmic resistivity of the cell, $j$ ($Am^{-2}$) is the electric current density and $\Delta E^{CP}$ (V) is the concentration (polarization) overpotential [50]. The ohmic resistance of a unit cell has contributions from the AEM and CEM, the dilute and concentrate compartments and from the spacers [51]. The ohmic potential constitutes the linear behavior of the current-voltage curve, while the overpotential is the deviation from linearity.

$\Delta E^{\text{CP}}$ describes the contribution of the concentration gradient in the boundary layers to the cell potential, and can be expressed by the Nernst equation [52]:

$$\Delta E^{\text{CP}} = \frac{\Delta g^{\text{CP}}}{|z_i|F} = \text{n}\frac{RT}{|z_i|F} ln\left(\frac{a_i^{\text{surf}}}{a_i^{\text{bulk}}}\right) \quad (2)$$

where $\Delta g^{\text{CP}}$ ($J \cdot mol^{-1}$) is the share of available work that is lost due to CP, $z_i$ is the charge number of ionic species $i$ as absolute value (i.e., z = 1 for chloride and fluoride), $F$ ($C \cdot mol^{-1}$) is the Faraday constant, n is the number of membranes used in the stack, $R$ ($J \cdot K^{-1} \cdot mol^{-1}$) is the universal gas constant, $T$ (K) is the solution temperature, $a_i^{\text{surf}}$ and $a_i^{\text{bulk}}$ ($mol^{-1} \cdot L$) are the surface and bulk activities of component $i$, respectively. The activity is defined as $a_i = \gamma_i c_i$, where $\gamma_i$ and $c_i$ are the activity coefficient and concentration of component $i$, respectively.

$\Delta E^{CP}$ can be quantified from a chronovoltametric sweep by extrapolating the linear behavior and determining the deviation between this linear contribution and the measured electric potential. Consequently, Eq. (2) can be solved for the activity ratio between the solution at the membrane surface and in the bulk:

$$\frac{a_i^{\text{surf}}}{a_i^{\text{bulk}}} = exp\left(\frac{\Delta E^{\text{CP}}}{\text{n}} \frac{|z_i|F}{RT}\right) \quad (3)$$

At the LCD, the left-hand term of Eq. (3) approaches zero. We call this novel technique for determining the LCD in ED the *boundary-layer* (*BL*) *method*.

## 3. Materials and methods

### 3.1. Materials

Commercial Selemion membranes (AGC Engineering Co., Ltd., Japan) of the type CMVN (common CEM) and ASVN (monovalent-selective AEM) were used. According to the technical specifications, both membranes have a thickness of 100 μm, CMVN has an area resistance of 2.0 $\Omega cm^2$ and ASVN has an area resistance of 4.0 $\Omega cm^2$ in 0.5 M NaCl. All membranes were stored in 0.1 M NaCl before the experiments; therefore, the area resistances are expected to be slightly higher than indicated by the suppliers for 0.5 NaCl. Woven silicone/polyester spacers with integrated gaskets were supplied by FumaTech (Germany), with a thickness of 470 μm, a mesh size of 800 μm, and a shadow effect of 0.33, according to supplier information. Solutions were prepared using demineralized water and technical grade NaCl, NaF, and $Na_2SO_4$ provided by Merck. Shenchen V6-6L peristaltic pumps (Baoding Shenchen Precision pump Co., Ltd., China) recirculated the solutions. For electrochemical measurements, the Gamry Interface 5000E potentiostat/galvanostat and respective Gamry software were used (Gamry Instruments, USA). Fluoride concentrations were measured using the inoLab® pH/ION 7320 benchtop meter with the F 800 DIN fluoride selective electrode. A total ionic strength adjustment buffer (TISAB) was purchased from Xylem WTW. Chloride concentrations were measured by silver nitrate titration ($AgNO_3$, 99 %, Aldrich), using an EasyPlus™ titrator by Mettler-Toledo (USA). Sulfate concentrations were measured by ion chromatography (IC, Metrohm 940 Professional IC Vario 1, Switzerland).

### 3.2. Experimental setup

An in-house-made cross-flow ED stack with an electrode area of 9 × 4 $cm^2$ was used. In each experiment, four cell pairs (4 AEMs and 5 CEMs) were stacked between the electrodes, and spacers were used between the membranes to facilitate solution flow and mixing. End spacers were used between the electrodes and the neighboring CEMs to establish a closed electrode rinse solution circuit. A batch of 500 mL 0.5 M $Na_2SO_4$ was used as electrode rinse solution at each electrode and circulated through the electrode compartments with a flow rate of 100 mL/min. The cell was run in batch mode, using 1 L of feed solution for the diluate and concentrate compartments. Each batch was stirred with a magnetic stirrer. A sketch of the setup with one unit cell (2 CEMs, 1 AEM) is shown in Fig. 3. A four-electrode configuration was used to measure current-voltage characteristics, where the working sense and counter sense were connected to the stack electrodes. Reference electrodes (mercury-sulfate electrodes provided by Gamry) were connected to the electrode rinse solution through salt bridges made with Agar and 0.5 M $Na_2SO_4$. The four-electrode setup eliminates the stack electrodes' contribution to the current-voltage characteristic, focusing the potential response on the membrane stack and its interfaces without accounting for electrode charge transfer resistance [53].

#### 3.2.1. Determining the limiting current density with the boundary-layer method

For the LCD experiments, 10 mM sodium chloride or 10 mM sodium sulfate were used as feed solutions and circulated at a flow rate of 100 mL/min, i.e., with a surface velocity of 2.2 cm/s through the ED stack equipped with four cell pairs. Amperodynamic sweeps were conducted, starting from open circuit potential (zero current drawn). The current was increased pulse-wise in 10 mA steps until the maximum voltage supplied by the potentiostat of 6 V was reached. Each current value was held for 30 s, while values for current and voltage were recorded every 0.25 s. The plot of current and voltage over time obtained from two repetitions with 10 mM NaCl is shown in Fig. 4a. The equivalent plot for 10 mM NaF can be found in Supplementary Material S1.

After 3/4 of the current step (the voltage value had stabilized), the voltage value was plotted against the respective current to obtain current-voltage characteristics from the experimental data. Current-voltage characteristics for 10 mM NaCl are shown in Fig. 4b for two repetitions. The dotted and dashed lines represent the linear extrapolation of the first five data points, i.e., the ohmic contribution to the cell potential. The deviation of the measured potential from the linear extrapolation gives the overpotential, as represented by Eq. (1). Fig. 4c visualizes the non-linear potential contribution as a function of the current density for 10 mM NaCl.

The obtained ratio $\frac{a_i^{\text{surf}}}{a_i^{\text{bulk}}}$ is an average for all nine diffusion boundary layers facing the dilute side. Fig. 4 d shows the apparent ratio of surface activity and bulk activity in the dilute compartment for 10 mM NaCl as a function of current density for two repetitions. The respective plots for NaF are given in Supplementary Material S1. The LCD value was reached when $\frac{a_i^{\text{surf}}}{a_i^{\text{bulk}}} < 0.01$, by definition.

The IS and CB methods were also used to determine the LCD, as described in Section 2. Fig. 5 shows the LCD determination with the IS and CB methods for two repetitions with 10 mM NaCl. The plots for LCD determination with the IS and CB methods for 10 mM NaF can be found in Supplementary Material S1. Note that our experiments' positive slope on the right-hand side of the plots is quasi-horizontal. Other groups have observed similar behavior [44,45].

The current-voltage curve of the mixture used as feed solution in the

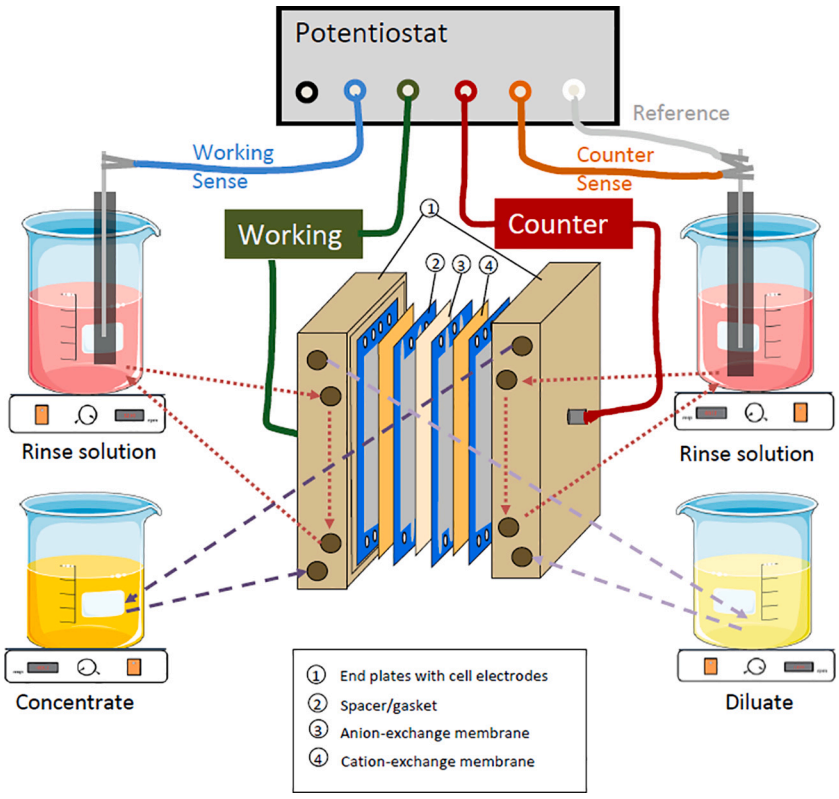


**Fig. 3.** Graphical description of the ED setup; A four-electrode setup was used for recording current-voltage curves, where the working and counter electrodes of the potentiostat were connected to the cell electrodes, working sense and counter sense/reference electrodes were in contact with the respective rinse solution via salt bridges. Note that the current-voltage curves were recorded for membrane stacks with four cell pairs, whereas the sketch illustrates a simplified setup with one cell pair.

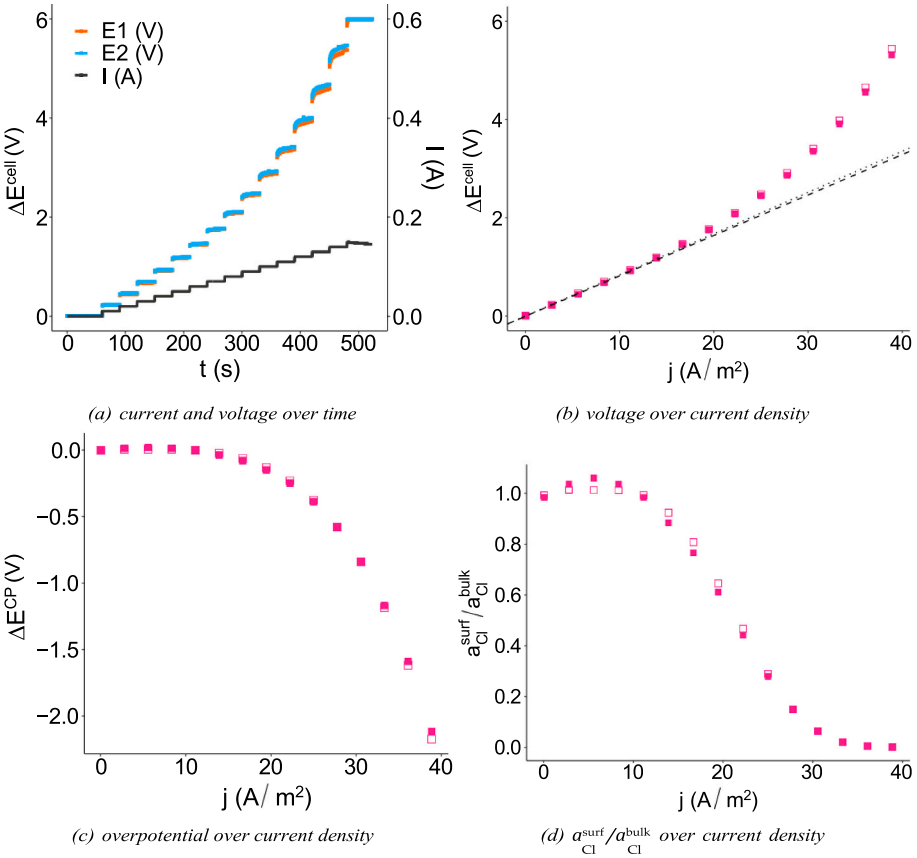


*(a) current and voltage over time*

*(b) voltage over current density*

*(c) overpotential over current density*

*(d) $a^{surf}_{Cl}/a^{bulk}_{Cl}$ over current density*

**Fig. 4.** Graphical description of the BL method for LCD determination for 10 mM NaCl: a potentiostat is connected to the ED cell, the current is increased stepwise, and the electric potential is recorded (a), the electric potential is plotted as a function of the current density (b), the overpotential $\Delta E^{CP}$ is determined as the current-voltage characteristic's deviation from linearity (c), and finally, the ratio of membrane surface activity to bulk activity is determined by inserting $\Delta E^{CP}$ into the Nernst equation (Eq. (2)). The LCD is reached by definition once $\frac{a_i^{surf}}{a_i^{bulk}} < 0.01$. E1 and E2 in (a) are the recorded electric potentials for two repetitions of the same experiment. In (b) to (d), the two repetitions are distinguished by hollow and full symbols. In (b), the dashed line corresponds to the linear extrapolation of the full symbols, while the dotted line corresponds to the hollow symbols.

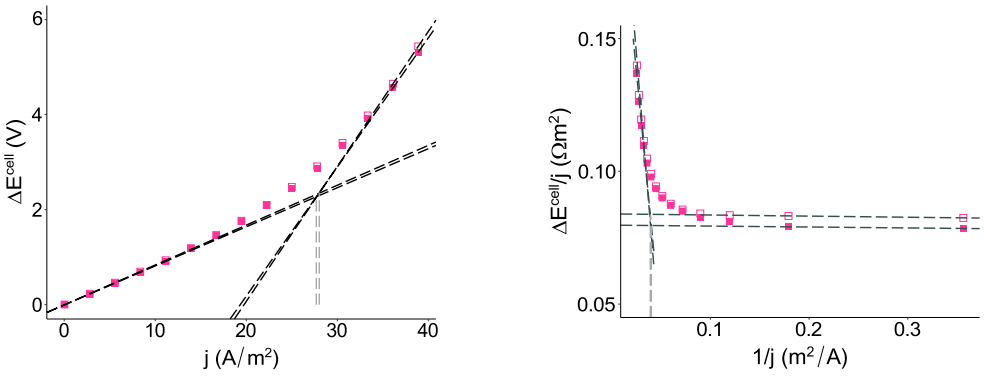


(a) Isaacson-Sonin method (b) Cowan-Brown method

**Fig. 5.** LCD of 10 mM NaCl solution circulated in the ED stack determined by (a) the Isaacson-Sonin method and (b) the Cowan-Brown method. For the IS method, the voltage is plotted over the current density and for the CB method, the voltage over the current density is plotted over the inverse current density. The hollow and full symbols distinguish two repetitions of the same experiment. The black lines represent the linear extrapolations of the right-hand and left-hand data points, where dashed lines correspond to full symbols, and dotted lines correspond to hollow symbols. As the dashed and dotted grey lines indicate, the intercept of the right- and left-hand side linear extrapolations determines the LCD.

desalination experiments (i.e., 10 mM NaCl, 10 mM NaF, and 1 M $Na_2SO_4$) was also compared. As expected, the measurement resulted in a straight line due to excess sodium sulfate.

### 3.2.2. Desalination experiments

ED was performed with a multi-ionic mixture of 10 mM NaCl, 10 mM NaF, and 1 M $Na_2SO_4$ to separate chloride and fluoride from the concentrated sulfuric solution. The applied current density was determined based on the LCD for NaCl and NaF. A relation between the current density and ionic fluxes inside the membrane is given by [54]:

$$j = F\sum_i |z_i| J_i^{\mathrm{mig}} \tag{4}$$

where $J_i^{\mathrm{mig}}$ is the migrative ion flux ($\mathrm{mol\cdot m^{-2}\cdot s^{-1}}$) of ionic species *i*. Eq. (4) suggests that the specific current density ascribed to the migrative transport of ionic species *i* is proportional to its valence $z_i$. Therefore, to apply the limiting current densities for NaCl and NaF and account for the current density assigned to the transport of $Na_2SO_4$ through the membrane, the optimal current density for the separation of chloride and fluoride from sulfate, $j_{\mathrm{opt}}$, was determined according to:

$$j_{\mathrm{opt}} = \left(j_{\mathrm{lim}}^{\mathrm{Cl^-}} + j_{\mathrm{lim}}^{\mathrm{F^-}}\right)\cdot 2 \tag{5}$$

Following on from Eq. (4), the divalent sulfate ions carry twice as much current as monovalent ions. Therefore, double the LCD value of the target ions must be provided when treating the multi-ionic mixture composed of sodium chloride, sodium fluoride, and sodium sulfate.

As a benchmark, desalination was also performed at a lower and a higher current density level, i.e.:

$$\begin{aligned} j_- &= 0.75\cdot j_{\mathrm{opt}} \\ j_+ &= 1.5\cdot j_{\mathrm{opt}} \end{aligned} \tag{6}$$

Desalination experiments lasted 300 min, whereas the LCD experiments lasted around 30 min. Therefore, $j_{\mathrm{opt}}$ corresponds to the optimum value for removing chloride and fluoride at the beginning of the ED treatment. With decreasing concentration in the dilute compartment, $j_{\mathrm{opt}}$ drops. The dynamic aspect of the LCD is considered when analyzing the results, where $j_{\mathrm{opt,t}}$ refers to the optimum current density at time step t. During the first hour of desalination, samples were taken from the dilute and concentrate batch every 10 min, for the second hour every 20 min, and for the next 3 h every 30 min. Samples were analyzed to determine the chloride, fluoride, and sulfate concentrations. In addition, the current density and voltage were recorded when taking a sample.

Sulfate concentrations were further fitted based on the ionic fluxes of chloride and fluoride. The fitting was carried out due to inaccuracies in the sulfate measurement, ascribed to the high dilution factor for the IC measurements. The chloride and fluoride fluxes were calculated based on their concentration change per time step [54]:

$$J_i \approx \frac{V}{A}\frac{c_i(n_t) - c_i(n_t - 1)}{t(n_t) - t(n_t - 1)} \tag{7}$$

where $V$ (L) is the solution volume on the diluate side, $A$ ($\mathrm{m^2}$) is the active area of the membrane, $c_i$ is the concentration of component *i* $\left(\mathrm{mol\cdot L^{-1}}\right)$, $n_t$ is the time step, and $t$ it the time (s). For each measurement, 7 mL samples were taken from the dilute and concentrate solution, leading to a total volume decrease of 105 mL in each batch during the experiment. This volume change was considered in the flux calculation. However, the water drag from the dilute to the concentrate compartment was neglected.

The fluxes of sulfate, chloride, and fluoride are linked by their transport numbers, where [55]:

$$\sum_i t_i = 1 \tag{8}$$

The transport number is the fraction of the electric current carried by an ionic species *i*. We assume perfectly selective anion-exchange membranes, where the sum of anion transport numbers is equal to unity, whereas the cation transport number is zero. The transport numbers of chloride and fluoride were calculated according to [54]:

$$t_i = \frac{F|z_i|J_i}{j} \tag{9}$$

$t_i$ is associated with the migrative flux of ions, $J_i^{\mathrm{mig}}$, and the total ion flux is the sum of migrative and diffusive terms, according to [54]:

$$J_i = J_i^{\mathrm{mig}} + J_i^{\mathrm{diff}} \tag{10}$$

The contribution of convection was neglected, which is common practice in the description of ED systems, justified by the relatively low water permeance of IEMs [56,57] and the fact that the migrative flux generally surpasses the convective flux significantly when an electric current is drawn [5,58]. The diffusive term was determined, and Eq. (10) was solved for the migrative term to find $t_{\mathrm{Cl}}$ and $t_{\mathrm{F}}$, which demonstrated that $J_i^{\mathrm{diff}}$ was negligible in the applied concentration range of chloride and fluoride. Therefore, $J_i$ was used in Eq. (9) rather than $J_i^{\mathrm{mig}}$. The transport number for sulfate was found through:

$$t_{SO_4^{2-}} = 1 - t_{Cl^-} - t_{F^-} \tag{11}$$

Eq. (9) was then solved for the ion flux of sulfate, neglecting the diffusive term of sulfate transport. Finally, the sulfate concentration in the dilute solution was estimated considering the measured starting concentration and using Eq. (7), which was solved numerically as:

$$c_{SO_4^{2-}}^{LC}(n_t) \approx c_{SO_4^{2-}}^{LC}(n_t - 1) - J_{SO_4^{2-}}\frac{A}{V}\left(t(n_t) - t(n_t - 1)\right) \tag{12}$$

### 3.3. Performance evaluation

The cumulative energy consumption, or work input $W$, for a given period of ED treatment is defined as:

$$W = \int_0^t \Delta E^{\text{cell}} I \mathrm{d}t \tag{13}$$

where $I$ is the electric current (A). The energy-specific transport rate of each anion is assessed as the concentration change of ion $i$ achieved per energy input:

$$J_i^E = \frac{V \Delta c_i}{W} \tag{14}$$

where $\Delta c_i$ is the change in ion concentration between two measurements. $J_i^E$ is the inverse of the more commonly used *specific energy consumption* [59] and more suitable when assessing the contributions of competing counter-ions to the energy requirement. The Gibbs free energy of separation, $\Delta G_{\text{mix}}$, defines the minimum energy expenditure for a certain separation (i.e., change in chemical potential) in a feed solution. As such, $\Delta G_{\text{mix}}$ corresponds to a thermodynamically reversible process, which can be envisioned as a batch ED setup with an applied voltage that is always infinitesimally larger than the equilibrium voltage and takes an infinitely long time. Excess energy is necessary to achieve a finite desalination rate (i.e., salt removal rate) for practical applications [60]. For separating NaCl, NaF, and $Na_2SO_4$ at constant pressure and temperature in an ED stack, the Gibbs free energy of separation is defined as:

$$\Delta G_{\text{mix}} = RTV \left[ \left( c^{HC}_{\text{NaCl}} ln \left( \frac{a^{LC}_{\text{NaCl}}}{a^{HC}_{\text{NaCl}}} \right) + c^{HC}_{\text{NaF}} ln \left( \frac{a^{LC}_{\text{NaF}}}{a^{HC}_{\text{NaF}}} \right) + c^{HC}_{\text{Na}_2\text{SO}_4} ln \left( \frac{a^{LC}_{\text{Na}_2\text{SO}_4}}{a^{HC}_{\text{Na}_2\text{SO}_4}} \right) \right] \tag{15}$$

The general expression for the Gibbs free energy of mixing is derived from [61] and can be consulted in the Supplementary Material. The Pitzer model, as described in [62], was used to estimate activity coefficients. The relevant coefficients for NaCl, NaF, and $Na_2SO_4$ are taken from [63]. The solution volume is calculated by subtracting the removed sample volume from the initial volume of the batch, not accounting for water transfer between the dilute, concentrate, and electrode compartments. We assume that the ions removed from the diluate are added to the concentrate and therefore calculate $c_i^{HC}$ from the concentration change in the diluate compartment.

To investigate the energy efficiency, $\eta$, the second law efficiency was determined, i.e., the ratio of the increase in available work attained by the products, $\Delta G_{\text{Cl,F}}$, to the maximum available useful work of the energy consumed, $W$ [64]:

$$\eta = \frac{\Delta G_{Cl,F}}{W} \cdot 100 \tag{16}$$

Since the treatment goal is to remove Cl and F, $\Delta G_{Cl,F}$ was used rather than $\Delta G_{\text{mix}}$, which is obtained by eliminating the last right-hand term from Eq. (15). Leakage of sulfate contributes to Eq. (16) as an energy loss.

We further assessed the separation efficiency between the target and competing sulfate ions. The transport number is often used to quantify the selectivity of a process or membrane for a specific ion. However, the transport number is proportional to the ion flux and, therefore, to the effective ionic concentration change over time (see Eq. (7)). Certainly, the total concentration change per time-step is higher for counter-ions with higher concentrations. To evaluate the relative difference in transport rate between two ions A and B of different concentrations, the separation efficiency, $S_B^A$, as introduced by Zhao et al. [65], is used:

$$S_B^A(t) = \frac{\left[\frac{c_B(t)}{c_B(0)}\right] - \left[\frac{c_A(t)}{c_A(0)}\right]}{\left[1 - \frac{c_B(t)}{c_B(0)}\right] + \left[1 - \frac{c_A(t)}{c_A(0)}\right]} \tag{17}$$

where $c_A(0)$ is the initial concentration of the target ion in the dilute compartment, $c_B(0)$ is the initial concentration of the competing counter-ion in the dilute compartment, $c_A(t)$ and $c_B(t)$ are the concentrations of $A$ and $B$ at time $t$, respectively. $S_B^A$ ranges from $-1$ (complete depletion of ion $B$) to 1 (complete depletion of ion $A$). To increase comparability with other studies, the selectivity $P_B^A = \frac{t_A/t_B}{c_A/c_B}$, which is often presented as a membrane property and commonly measured in equimolar mixtures of counter-ions [5], was also determined and is given in the Supplementary Material S4.

## 4. Results and discussion

The ED process must be balanced regarding removal rates of target ions, leakage of competing ions, separation efficiency, and energy input according to the treatment goals. The trade-off between removal rate and energy input is a target for optimization in ED. In addition, for multi-ionic mixtures, a higher removal rate of target ions is typically accompanied by increased leakage of competing counter-ions. The separation efficiency classifies which of the competing ions shows a relatively higher increase in transport rate with increasing current density. Consequently, the ratio of transport rates is controlled by the current density, i.e., the intensity of CP. The results of this experimental study elucidate whether the transport ratio of target ions versus competing counter-ions is optimal when working at the LCD of the target ions.

Table 1 presents an overview of the experimental results and analyses conducted to compare the ED performance at the three current density levels. In the following, these results are discussed in detail.

### 4.1. Determination of LCD

The LCD was determined by the BL method described in Section 3.2.1 and compared to the IS and CB methods. Values for the LCD obtained by the different methods are presented in Table 2. Note that there is no margin of error for the BL method, as this method gives discrete values, which were the same in the two repetitions for all measurements.

The BL method results in considerably higher values for the LCD than the IS and CB methods, which give similar values. This is consistent with the difference in the underlying definitions of LCD, where the BL method defines the LCD as when the surface activity of ion $i$ becomes negligible compared to the bulk activity, as discussed in Section 2. However, this definition has an ambiguity as we need to define at which $a_{\text{surf}}/a_{\text{bulk}}$ value $a_{\text{surf}}$ becomes negligible. We consider $a_{\text{surf}}/a_{\text{bulk}} < 0.01$ as an adequate and practical criterion. For higher accuracy, the data density can be enhanced around the LCD by decreasing the step size in the amperodynamic sweeps.

Similarly, the IS and CB methods are known to be sensitive to the

**Table 1**
Comparison of the ED performance after 5 h treatment at $j_-$, $j_{opt}$ and $j_+$.

| | | $j$ (A/m$^2$) | | |
|---|---|---|---|---|
| | | 100 | 130 | 200 |
| Removal (%) | $Cl^-$ | <90 ± 1[a] | <86 ± 2[a] | <87 ± 1[a] |
| | $F^-$ | 23 ± 4 | 98 ± 1 | 98 ± 1 |
| | $SO_4^{2-}$ | 11 ± 1 | 19 ± 2 | 23 ± 7 |
| $J_i^E$ (mmol/J) | $Cl^-$ | 10.89 ± 0.75 | 4.37 ± 0.03 | 1.76 ± 0.63 |
| | $F^-$ | 0.90 ± 0.19 | 1.45 ± 0.08 | 0.37 ± 0.05 |
| | $SO_4^{2-}$ | 47.57 ± 0.38 | 15.14 ± 0.30 | 6.43 ± 0.17 |
| $\Delta G_{\text{mix}}$ (kJ) | $Cl^-$ | 0.12 ± 0.01 | 0.12 ± 0.02 | 0.14 ± 0.05 |
| | $F^-$ | 0.01 ± 0.00 | 0.17 ± 0.02 | 0.16 ± 0.00 |
| | $SO_4^{2-}$ | 0.34 ± 0.03 | 0.46 ± 0.00 | 0.80 ± 0.07 |
| $\eta$ (%) | | 1.52 ± 0.28 | 0.93 ± 0.00 | 0.18 ± 0.16 |
| $S^{Cl^-}_{SO_4^{2-}}$ | | 0.91 ± 0.01 | 0.93 ± 0.00 | 0.88 ± 0.00 |
| $S^{F^-}_{SO_4^{2-}}$ | | 0.30 ± 0.04 | 0.81 ± 0.00 | 0.73 ± 0.00 |

[a] Last value within detection limit.

**Table 2**
Comparison between the LCD obtained with the BL, IS and CB methods.

| | Boundary-layer ($A/m^2$) | Isaacson-Sonin ($A/m^2$) | Cowan-Brown ($A/m^2$) |
|---|---|---|---|
| NaCl | 36.10 | 27.84 ± 0.16 | 27.66 ± 0.34 |
| NaF | 30.56 | 22.05 ± 0.09 | 21.78 ± 0.16 |

density of experimental data for the high-current-density tangents. To quantify this sensitivity, the LCD was determined with the IS and CB methods using the two, three, and four last data points recorded with the amperodynamic sweep. Note that for the IS method, these are the last two to four data points on the right side of Fig. 5a, while for the CB method, they are on the left side of Fig. 5b since the x-axis represents $1/j$. Table 3 shows the LCD for NaCl and NaF with the error margin of two repetitions.

While the IS and CB methods attained similar values for the LCD, the LCD varied considerably for both methods depending on the data points included in the graphical determination. For both chloride and fluoride, the value decreased by more than 1 $A/m^2$ when one more data point was considered. The choice of data points for the high-current tangent is not obvious.

The three current density levels for the desalination experiments were found by inserting the LCD determined by the BL method into Eq. (6), resulting in values of $j_- = 100$ $A/m^2$, $j_{opt} = 130$ $A/m^2$, and $j_+ = 200$ $A/m^2$. When using the LCD values suggested by the IS and CB methods, $j_{opt}$ becomes approximately 100 $A/m^2$ (99.78 $A/m^2$ with the IS method and 98.88 $A/m^2$ with the CB method). Notably, $j_-$ according to the BL method coincides with $j_{opt}$ determined by the IS and CB methods. Consequently, the ED performance at the optimum current density as determined by the BL method is compared to each one higher and one lower control value and concomitantly to the optimum value determined by the IS and CB methods.

### 4.2. Desalination experiments

Fig. 6 shows the removal rates ($c/c(0)$) of chloride, fluoride, and sulfate, respectively, in the dilute compartment as functions of time. Each experiment was run two times, and each data point is the mean value of two repetitions within the respective error bar. Note that the applied currents correspond to the initial concentrations of chloride and fluoride and are not adjusted to the concentration decrease during the experiment. Chloride, plotted in Fig. 6a, has the highest transport rate of the three anions. The sensitivity of the concentration analysis only allowed us to track the chloride concentration to about 10 % of its starting value before the concentration fell below the detection limit. When applying 100 $A/m^2$ ($j_-$), chloride was depleted to under 10 % of its starting concentration after 3 h of treatment. For both 130 $A/m^2$ ($j_{opt}$) and 200 $A/m^2$ ($j_+$), the threshold was reached after 100 min. The desalination curves for chloride at 130 $A/m^2$ and 200 $A/m^2$ are nearly the same, with a slightly increased transport rate at 200 $A/m^2$ in the first 2/3 of the process. However, after chloride is depleted to around 20 % of its starting concentration, the desalination curves flatten, and the curves at $j_{opt}$ and $j_+$ converge. The flattening curve indicates that once the chloride concentration reaches approximately 2 mM, the transport of

**Table 3**
LCD values obtained with the IS and CB methods for ED with 10 mM NaCl and 10 mM NaF.

| LCD ($A/m^2$) | 2-Point tangent | | 3-Point tangent | | 4-Point tangent | |
|---|---|---|---|---|---|---|
| | IS | CB | IS | CB | IS | CB |
| NaCl | 27.84 ± 0.16 | 27.66 ± 0.34 | 26.66 ± 0.12 | 26.41 ± 0.31 | 25.49 ± 0.12 | 25.15 ± 0.32 |
| NaF | 22.05 ± 0.09 | 21.78 ± 0.16 | 20.86 ± 0.01 | 20.49 ± 0.06 | 19.61 ± 0.03 | 19.10 ± 0.05 |

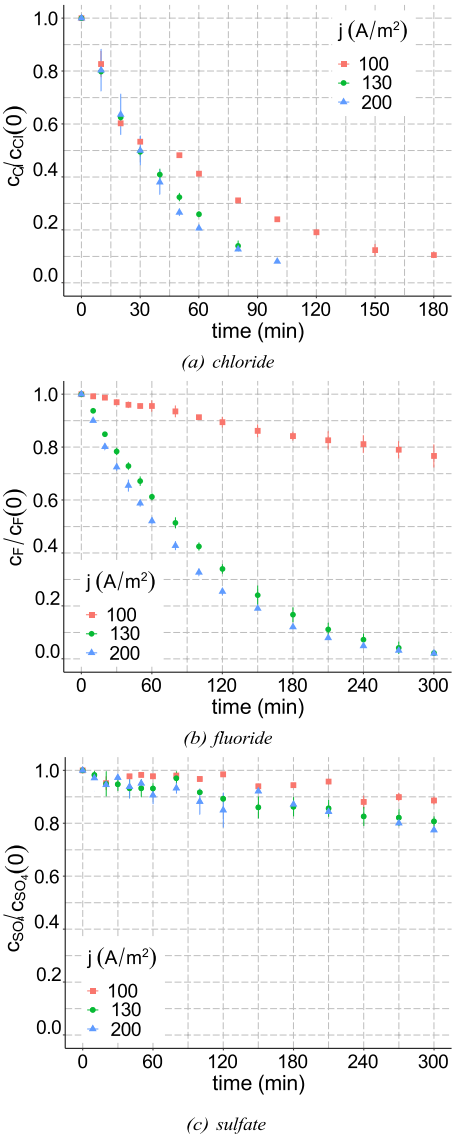


**Fig. 6.** ED Desalination curves with ternary mixtures of 10 mM chloride, 10 mM fluoride, and 1 M sulfate at different current densities.

chloride ions to the membrane becomes the rate-determining step, making the transport rate independent of the current density. The same behavior can be observed for $j_-$. Removal of chloride passed 2 mM is therefore associated with increased energy cost. This can be ascribed to the increasing $j_{applied}/j_{opt,t}$ ratio during the experiment. Continuous operation of the ED cell, multi-stage operation, or dynamic control of the current to match the target ion concentration can counteract the growing energy inefficiency [60].

The fluoride transport rate is considerably lower compared to chloride. As seen in Fig. 6b, fluoride is depleted after 300 min of ED at 130 $A/m^2$ and 200 $A/m^2$. Similar to chloride, a retardation of the slope is observed around 2 mM, and the plots for $j_{opt}$ and $j_+$ converge. Remarkably, at 100 $A/m^2$, the fluoride removal rate was only 23 % after 5 h of desalination. These results imply that the fluoride transport rate is the controlling factor for removing chloride and fluoride from the sulfate solution. While the fluoride transport was impractically slow at $j_-$, it increased significantly when stepping the current up to $j_{opt}$, corresponding to the LCD suggested by the BL method. Even though fluoride has a lower LCD than fluoride in the single-salt measurements presented in Section 4.1, chloride was depleted before fluoride at $j_-$. This can be ascribed to the favorable ionic properties of chloride compared to

fluoride and sulfate, like a lower hydrated size and higher diffusivity [5]. Therefore, chloride transports a larger charge share when operating below the current corresponding to the LCD for chloride and fluoride. However, when increasing the current to $j_{opt}$, the mass transport of chloride takes on its maximum value where it is limited by diffusion, allowing fluoride to transport more charge across the cell and reach its maximum transport rate. A further increase to $j_+$ did not result in a similar mass transport enhancement. However, the improved transport rate of fluoride was accompanied by doubling the sulfate leakage, as seen in Fig. 6c. The sulfate leakage was around 10 % at 100 A/m$^2$ and around 20 % at 130 A/m$^2$ and 200 A/m$^2$.

As described in Section 3.2.2, the sulfate concentration was also estimated through the fluxes of chloride and fluoride and the relation $t_{Cl^-} + t_{F^-} + t_{SO_4^{2-}} = 1$. The modeled sulfate concentrations are presented in Fig. 7 alongside the mean measured concentrations for the three current density levels. The model shows reasonable conformity with the experimental data despite the simplifications of assuming perfectly selective AEMs and neglecting convection and the back-diffusion of sulfate. For assessing the performance parameters, the sulfate concentration provided by the model was used as the strong fluctuations of the measured values lead to inconsistencies in the further data processing.

Fig. 8 compares the energy-specific transport rates determined by Eq. (14) for chloride, fluoride, and sulfate at the three current density levels. The values represent an average over the whole duration of the experiment. The complete energy-specific transport rate profiles can be found in Supplementary Material S2. For chloride and sulfate, the energy-specific transport rate decreased with current density, while fluoride exhibits a higher transport rate at 130 A/m$^2$ than at 100 A/m$^2$. The particular behavior of fluoride can be ascribed to the significantly increased transport rate when stepping the current density up from $j_-$ to $j_{opt}$ (see Fig. 6b). Sulfate has the highest energy-specific transport rate among the competing anions due to its abundance in the solution. In contrast, fluoride has the lowest energy-specific transport rate due to its low concentration compared to sulfate and disadvantageous properties for transport across the membranes compared to chloride. Figs. S.3 to S.5 in Supplementary Material show that the energy-specific transport rate decreases during the experiments for chloride and fluoride and increases for sulfate. The decreasing energy efficiency can again be ascribed to the increasing $j_{applied}/j_{opt,t}$ ratio during the experiment. As seen in Fig. 8, $J^E_{Cl^-}$ decreased by approximately a factor of 2.5 between each current step. Between 100 A/m$^2$ and 130 A/m$^2$, $J^E_{F^-}$ increased by a factor of 1.6 while $J^E_{SO_4^{2-}}$ decreased by a factor of 3.4. For the second current step, $J^E_{F^-}$ and $J^E_{SO_4^{2-}}$ decreased by factors 3.9 and 2.4, respectively. Consequently, stepping the current up from $j_-$ to $j_{opt}$ significantly cut the energy-specific transport rate of sulfate while enhancing energy-specific

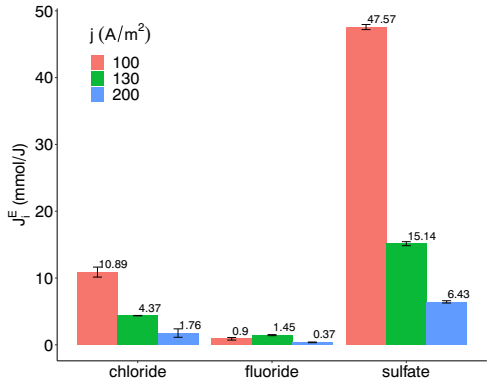


**Fig. 8.** Energy-specific chloride, fluoride, and sulfate transport rate at different current density levels as an average over the experiment duration.

fluoride transport. In contrast, increasing the current to 200 A/m$^2$ substantially restricted $J^E_{F^-}$. Therefore, among the three current densities, $j_{opt}$ seems most suited for the simultaneous removal of chloride and fluoride. Fig. 8 also reaffirms the slow fluoride transport as the bottleneck for halogen removal.

Fig. 9 shows the energy input as a function of chloride and fluoride removal rates at the three current levels. Up to 50 % removal, the relation between removal and work input was approximately linear. For removal beyond 50 %, the work requirement increased exponentially. At $j_-$, $j_{opt}$, and $j_+$, the work required to remove close to 90 % chloride was approximately 5 kJ, 10 kJ, and 50 kJ, respectively. At $j_-$, fluoride was removed by around 25 % at an energy expenditure of circa 8 kJ. At 130 A/m$^2$ and 200 A/m$^2$, the work input for close to 100 % fluoride removal was 30 kJ and 150 kJ, respectively. Consequently, the energy requirement for depletion tripled between $j_{opt}$ and $j_+$ for both target ions. Since the time required for the removal of chloride and fluoride was similar at $j_{opt}$ and $j_+$, the practical maximum current must lie between $j_-$ and $j_{opt}$.

Fig. 10 shows the Gibbs free energy for chloride, fluoride, and sulfate, as calculated with Eq. (15). For chloride, $\Delta G$ was similar at all current levels, reflecting that a similar chemical potential change was achieved. The same is true for fluoride at $j_+$ and $j_{opt}$, while $\Delta G_{NaF}$ at $j_-$ was 16 times lower, corresponding with the poor transport rate at that current density. $\Delta G_{Na_2SO_4}$ was around four times higher than $\Delta G_{NaCl}$ at 130 A/m$^2$, which can be ascribed to its high concentration in the solution. While the Gibbs energy remained nearly constant for NaCl and NaF between $j_{opt}$ and $j_+$, it almost doubled for sulfate separation. These results highlight the transport limitations for fluoride and chloride caused by depletion in the boundary layer. The increased current predominantly resulted in enhanced charge transfer through sulfate ions. Eq.

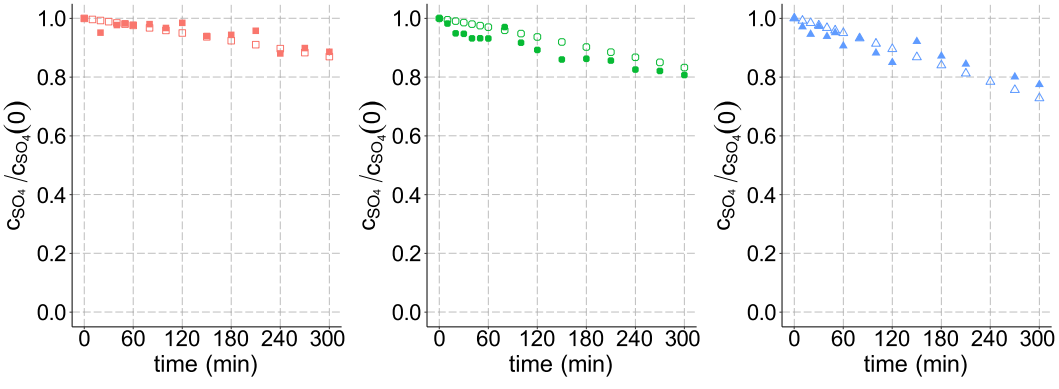


*(a) 100 A/m²* *(b) 130 A/m²* *(c) 200 A/m²*

**Fig. 7.** Experimentally determined (full symbols) and modeled (hollow symbols) sulfate removal rate in ED desalination at different current density levels.

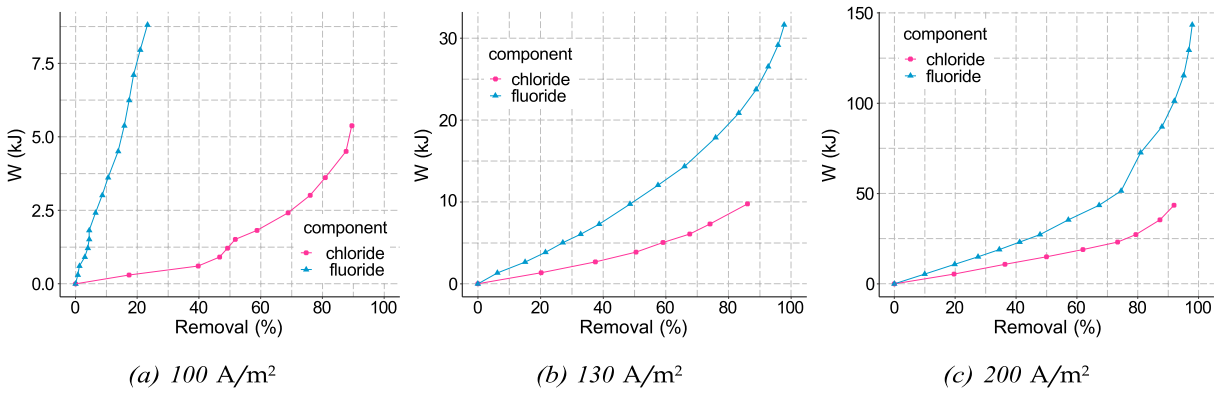


**Fig. 9.** Work input as a function of removal rate for chloride and fluoride at the different current density levels. Note the different magnitudes of the y-axes. Symbols represent experimental data, and lines are added to guide the eye.

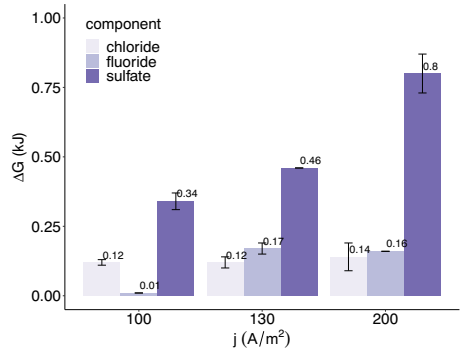


**Fig. 10.** Gibbs energy per component at the three current density levels.

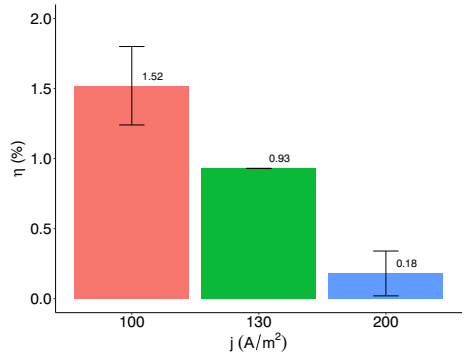


**Fig. 11.** Second law efficiency determined after 5 h of ED treatment at the three current density levels.

(16) defines energy efficiency as the ratio of the Gibbs free energy of fluoride and chloride to the total consumed work in the system. The results for the three current levels are shown in Fig. 11 as the average of two repetitions with the respective error bars. In accordance with the increased excess energy, $\eta$ dropped from approximately 1.5 % at 100 A/m$^2$ to 1 % at 130 A/m$^2$ and 0.2 % at 200 A/m$^2$. While the loss of energy efficiency between $j_-$ and $j_{opt}$ was accompanied by a significant improvement in fluoride removal rate, the decrease between $j_{opt}$ and $j_+$ was not justified by a corresponding gain in fluoride removal. Consequently, $j_{opt}$ is suggested as the preferable current level allowing high mass transport of target ions while limiting the excess energy.

The separation efficiency was determined according to Eq. (17). Separation efficiencies between chloride and sulfate and between fluoride and sulfate at the three current density levels are presented in

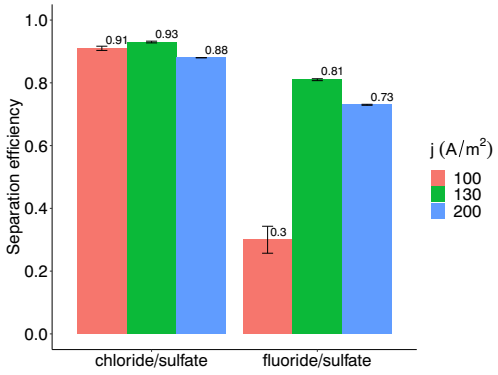


**Fig. 12.** Separation efficiencies $S_S^{Cl}$ and $S_S^F$ at different current density levels.

Fig. 12 as averages through the experiment with the respective error bars. The full profiles, presented in Supplementary Material S3, show a decreasing trend over time in accordance with the increasing $j_{applied}/j_{opt,t}$ ratio. In all cases, the process was selective for chloride and fluoride over sulfate (separation efficiencies > 0). However, the separation efficiency between fluoride and sulfate was as low as 0.30 at $j_-$, increased to 0.81 when increasing the current density to $j_{opt}$, and dropped to 0.73 with a further increase to $j_+$. For chloride and sulfate, the difference in separation efficiency at different operating current densities was less distinct. Notably, the separation efficiency was highest for both target ions at $j_{opt}$. The selectivities between chloride and sulfate and between fluoride and sulfate, presented in Fig. S.8 as averages through the experiment, show similar trends, with a maximum of 24.47 for chloride over sulfate and 10.02 for fluoride over sulfate. These results support our hypothesis that the ion-specific LCD must be considered for optimum ion selectivity in the ED of multi-ionic mixtures. Follow-up studies will be performed to elucidate the influence of the solution composition, i.e., the ratio of target ions to competing counter-ions, on the process selectivity.

## 5. Conclusion

This work investigated the ion-specific limiting current density (LCD) as a selectivity promoter in the Electrodialysis (ED) of multi-ionic mixtures. A new method called the boundary-layer method (BL) was presented to determine the LCD for binary salt solutions in an ED setup. The method takes advantage of the Nernst equation. Extrapolating the ion-specific LCD to multi-ionic mixtures allows for identifying the optimal operating current regarding the mass transfer of target ions while limiting excess energy consumption. ED was performed on mixtures of 10 mM NaCl, 10 mM NaF, and 1 M $Na_2SO_4$ with the goal of removing chloride and fluoride. The experimental results suggested 130

$A/m^2$ as the optimum current density ($j_{opt}$) for this application, while 100 $A/m^2$ and 200 $A/m^2$ were used as lower ($j_-$) and higher ($j_+$) control values, respectively. The lower control value corresponds to the ion-specific LCD determined with the Isaacson-Sonin (IS) and Cowan-Brown (CB) methods.

The following points summarize our main findings:

- Chloride was depleted ahead of fluoride due to its favorable transport properties and ion characteristics. Therefore, the fluoride transport rate was the controlling factor for removing chloride and fluoride from the base electrolyte solution.
- While fluoride removal was only 23 % after 5 h of ED at $j_-$, complete depletion of fluoride was observed during the same treatment time at $j_{opt}$. A further increase to $j_+$ did not result in a significant enhancement of target ion removal, which suggests that the removal rates of chloride and fluoride were limited by diffusion in the boundary layer.
- The work input and energy efficiency for 5 h of ED increased with current, as a larger current leads to higher efficiency losses. However, between $j_-$ and $j_{opt}$, the excess work input and lower energy efficiency were justified by the enhanced fluoride removal rate, which was not the case for $j_+$.
- The separation efficiency for removal of fluoride over sulfate increased significantly when stepping the current density up from 100 $A/m^2$ to 130 $A/m^2$, and dropped again at 200 $A/m^2$.

Among the three current density levels, $j_{opt}$ was favorable for the simultaneous removal of chloride and fluoride. Our results imply that the ion-specific LCD is a critical parameter to optimize separation efficiency for removing dilute target ions from concentrated solutions with ED. Furthermore, the BL method was better suited to finding the optimum current than the CB and IS methods. To further restrict the optimum current density, more experiments must be conducted between $j_-$ and $j_{opt}$. Future research could be directed towards a more thorough theoretical formulation of the transport phenomena in the laminar boundary layer and membranes to identify the main drivers for selectivity among counter-ions and maximize current efficiency.

## CRediT authorship contribution statement

Pauline Zimmermann: Conceptualization, Methodology, Formal analysis, Validation, Investigation, Writing - original draft, Visualization. Önder Tekinalp: Writing - Review & editing. Simon Birger Byremo Solberg: Methodology, Writing - Review & editing. Øivind Wilhelmsen: Supervision, Writing - Review & editing. Liyuan Deng: Writing - Review & editing. Odne Stokke Burheim: Conceptualization, Supervision, Writing - Review & editing. All authors have read and agreed to the published version of the manuscript.

## Declaration of competing interest

The authors declare that they have no known competing financial interests or personal relationships that could have appeared to influence the work reported in this paper.

## Data availability

Data will be made available on request.

## Acknowledgements

The authors acknowledge the financial support from the Research Council of Norway (RCN-BIA) through the PRICE project (No. 294543) and the support from the Norwegian Micro- and Nano-Fabrication Facility, NorFab (No. 295864). The authors also thank S. Menegatti and other colleagues from Boliden Odda AS for technical assistance. ØW acknowledges funding from the Research Council of Norway (RCN), the Center of Excellence Funding Scheme, Project No. 262644, PoreLab.

## Appendix A. Supplementary data

Supplementary data to this article can be found online at https://doi.org/10.1016/j.desal.2023.116613.

## References

[1] E. Drioli, E. Fontananova, Membrane technology and sustainable growth, Chem. Eng. Res. Des. 82 (12) (2004) 1557–1562, https://doi.org/10.1205/cerd.82.12.1557.58031.
[2] S. Al-Amshawee, M.Y.B.M. Yunus, A.A.M. Azoddein, D.G. Hassell, I.H. Dakhil, H. A. Hasan, Electrodialysis desalination for water and wastewater: a review, Chem. Eng. J. 380 (2020), 122231, https://doi.org/10.1016/j.cej.2019.122231.
[3] P. Pillai, S. Dharaskar, S. Pandian, H. Panchal, Overview of fluoride removal from water using separation techniques, Environ. Technol. Innov. 21 (2021), 101246, https://doi.org/10.1016/j.eti.2020.101246.
[4] P. Zimmermann, O.̈ Tekinalp, L. Deng, K. Forsberg, Ø. Wilhelmsen, O. Burheim, Electrodialysis in hydrometallurgical processes, in: M. Luby (Ed.), Rare Metal Technology 2020, Springer, 2020, pp. 159–167, https://doi.org/10.1007/978-3-030-36758-9_15.
[5] T. Luo, S. Abdu, M. Wessling, Selectivity of ion exchange membranes: a review, J. Membr. Sci. 555 (2018) 429–454, https://doi.org/10.1016/j.memsci.2018.03.051.
[6] F.E. Ahmed, A. Khalil, N. Hilal, Emerging desalination technologies: current status, challenges and future trends, Desalination 517 (2021), 115183, https://doi.org/10.1016/j.desal.2021.115183.
[7] P. Xu, M. Capito, T.Y. Cath, Selective removal of arsenic and monovalent ions from brackish water reverse osmosis concentrate, J. Hazard. Mater. 260 (2013) 885–891, https://doi.org/10.1016/j.jhazmat.2013.06.038.
[8] P. Zimmermann, S.B.B. Solberg, O.̈ Tekinalp, J.J. Lamb, Ø. Wilhelmsen, L. Deng, O.S. Burheim, Heat to hydrogen by RED—reviewing membranes and salts for the RED heat engine concept, Membranes 12 (1) (2022) 48, https://doi.org/10.3390/membranes12010048.
[9] H. Meng, D. Deng, S. Chen, G. Zhang, A new method to determine the optimal operating current (Ilim') in the electrodialysis process, Desalination 181 (1-3) (2005) 101–108, https://doi.org/10.1016/j.desal.2005.01.014.
[10] P.D. Lugo Lkecki, B. Anet, S.J. Metz, K. Nijmeijer, M. Wessling, Transport limitations in ion exchange membranes at low salt concentrations, J. Membr. Sci. 346 (1) (2010) 163–171, https://doi.org/10.1016/j.memsci.2009.09.033.
[11] N. Pis'menskaya, V. Nikonenko, N. Mel'nik, G. Pourcelli, G. Larchet, Effect of the ion-exchange-membrane/solution interfacial characteristics on the mass transfer at severe current regimes, Rus. J. Electrochem. 48 (6) (2012) 610–628, https://doi.org/10.1134/S1023193512060092.
[12] A. Nakayama, Y. Sano, X. Bai, K. Tado, A boundary layer analysis for determination of the limiting current density in an electrodialysis desalination, Desalination 404 (2017) 41–49, https://doi.org/10.1016/j.desal.2016.10.013.
[13] H.-J. Lee, H. Strathmann, S.-H. Moon, Determination of the limiting current density in electrodialysis desalination as an empirical function of linear velocity, Desalination 190 (1-3) (2006) 43–50, https://doi.org/10.1016/j.desal.2005.08.004.
[14] A. Peers, Electrodialysis using ion-exchange membranes II. Demineralization of solutions containing amino-acids, J. Appl. Chem. 8 (1) (1958) 59–67, https://doi.org/10.1002/jctb.5010080110.
[15] V. Geraldes, M.D. Afonso, Limiting current density in the electrodialysis of multiionic solutions, J. Membr. Sci. 360 (1-2) (2010) 499–508, https://doi.org/10.1016/j.memsci.2010.05.054.
[16] B.S.M. Ali, A. Mnif, B. Hamrouni, Modelling of the limiting current density of an electrodialysis process by response surface methodology, Ionics 24 (2) (2018) 617–628, https://doi.org/10.1007/s11581-017-2214-7.
[17] A. Gorobchenko, S. Mareev, V. Nikonenko, Mathematical modeling of monovalent permselectivity of a bilayer ion-exchange membrane as a function of current density, Int. J. Mol. Sci. 23 (9) (2022) 4711, https://doi.org/10.3390/ijms23094711.
[18] V. Zabolotsky, A. Achoh, K. Lebedev, S. Melnikov, Permselectivity of bilayered ionexchange membranes in ternary electrolyte, J. Membr. Sci. 608 (2020), 118152, https://doi.org/10.1016/j.memsci.2020.118152.
[19] Z. Luo, D. Wang, D. Zhu, J. Xu, H. Jiang, W. Geng, W. Wei, Z. Lian, Separation of fluoride and chloride ions from ammonia-based flue gas desulfurization slurry using a two-stage electrodialysis, Chem. Eng. Res. Des. 147 (2019) 73–82.
[20] H.-F. Xiao, Q. Chen, H. Cheng, X.-M. Li, W.-M. Qin, B.-S. Chen, D. Xiao, W.-M. Zhang, Selective removal of halides from spent zinc sulfate electrolyte by diffusion dialysis, J. Membr. Sci. 537 (2017) 111–118, https://doi.org/10.1016/j.memsci.2017.05.009.
[21] M. Stevens, B. Batlokwa, Removal of excess toxic chloride and fluoride anions from wastewater employing eggshells waste remains, Int. J. Adv. Eng. Res. Sci. 5 (9) (2018), 264267, https://doi.org/10.22161/ijaers.5.9.9.
[22] M. Reig, C. Valderrama, O. Gibert, J.L. Cortina, Selectrodialysis and bipolar membrane electrodialysis combination for industrial process brines treatment:

monovalent-divalent ions separation and acid and base production, Desalination 399 (2016) 88–95, https://doi.org/10.1016/j.desal.2016.08.010.
[23] M. Reig, X. Vecino, M. Hermassi, C. Valderrama, O. Gibert, J. Cortina, Integration of selectrodialysis and solvent-impregnated resins for zn (II) and cu (II) recovery from hydrometallurgy effluents containing as (V), Sep. Purif. Technol. 229 (2019), 115818, https://doi.org/10.1016/j.seppur.2019.115818.
[24] J. Liao, Q. Chen, N. Pan, X. Yu, X. Gao, J. Shen, C. Gao, Amphoteric blend ion-exchange membranes for separating monovalent and bivalent anions in electrodialysis, Sep. Purif. Technol. 242 (2020), 116793, https://doi.org/10.1016/j.seppur.2020.116793.
[25] P. Goel, E. Bhuvanesh, P. Mandal, V.K. Shahi, A. Bandyopadhyay, S. Chattopadhyay, Di-quaternized graphene oxide based multi-cationic cross-linked monovalent selective anion exchange membrane for electrodialysis, Sep. Purif. Technol. 276 (2021), 119361, https://doi.org/10.1016/j.seppur.2021.119361.
[26] S. Mulyati, R. Takagi, A. Fujii, Y. Ohmukai, H. Matsuyama, Simultaneous improvement of the monovalent anion selectivity and antifouling properties of an anion exchange membrane in an electrodialysis process, using polyelectrolyte multilayer deposition, J. Membr. Sci. 431 (2013) 113–120, https://doi.org/10.1016/j.memsci.2012.12.022.
[27] D. Golubenko, A. Yaroslavtsev, Effect of current density, concentration of ternary electrolyte and type of cations on the monovalent ion selectivity of surface-sulfonated graft anion-exchange membranes: modelling and experiment, J. Membr. Sci. 635 (2021), 119466, https://doi.org/10.1016/j.memsci.2021.119466.
[28] M. Ahmad, C. Tang, L. Yang, A. Yaroshchuk, M.L. Bruening, Layer-by-layer modification of aliphatic polyamide anion-exchange membranes to increase cl-/SO42- selectivity, J. Membr. Sci. 578 (2019) 209–219, https://doi.org/10.1016/j.memsci.2019.02.018.
[29] Y. Zhao, Y. Li, S. Yuan, J. Zhu, S. Houtmeyers, J. Li, R. Dewil, C. Gao, B. Van der Bruggen, A chemically assembled anion exchange membrane surface for monovalent anion selectivity and fouling reduction, J. Mater. Chem. A 7 (11) (2019) 6348–6356, https://doi.org/10.1039/C8TA11868J.
[30] Z. Zheng, P. Xiao, H. Ruan, J. Liao, C. Gao, B.V.D. Bruggen, J. Shen, Mussel-inspired surface functionalization of AEM for simultaneously improved monovalent anion selectivity and antibacterial property, Membranes 9 (3) (2019) 36, https://doi.org/10.3390/membranes9030036.
[31] Y. Zhao, H. Liu, K. Tang, Y. Jin, J. Pan, B.V. der Bruggen, J. Shen, C. Gao, Mimicking the cell membrane: bio-inspired simultaneous functions with monovalent anion selectivity and antifouling properties of anion exchange membrane, Sci. Rep. 6 (1) (2016) 1–13, https://doi.org/10.1038/srep37285.
[32] J. Pan, J. Ding, R. Tan, G. Chen, Y. Zhao, C. Gao, B. Van der Bruggen, J. Shen, Preparation of a monovalent selective anion exchange membrane through constructing a covalently crosslinked interface by electro-deposition of polyethyleneimine, J. Membr. Sci. 539 (2017) 263–272, https://doi.org/10.1016/j.memsci.2017.06.017.
[33] Y. Zhao, J. Zhu, J. Ding, B. Van der Bruggen, J. Shen, C. Gao, Electric-pulse layerby-layer assembled of anion exchange membrane with enhanced monovalent selectivity, J. Membr. Sci. 548 (2018) 81–90, https://doi.org/10.1016/j.memsci.2017.11.007.
[34] H. Liu, H. Ruan, Y. Zhao, J. Pan, A. Sotto, C. Gao, B. Van der Bruggen, J. Shen, A facile avenue to modify polyelectrolyte multilayers on anion exchange membranes to enhance monovalent selectivity and durability simultaneously, J. Membr. Sci. 543 (2017) 310–318, https://doi.org/10.1016/j.memsci.2017.08.072.
[35] Ö. Tekinalp, P. Zimmermann, O.S. Burheim, L. Deng, Designing monovalent selective anion exchange membranes for the simultaneous separation of chloride and fluoride from sulfate in an equimolar ternary mixture, J. Membr. Sci. 666 (2023), 121148, https://doi.org/10.1016/j.memsci.2022.121148.
[36] N. Kabay, Ö. Arar, S. Samatya, Ü. Yüksel, M. Yüksel, Separation of fluoride from aqueous solution by electrodialysis: effect of process parameters and other ionic species, J. Hazard. Mater. 153 (1-2) (2008) 107–113, https://doi.org/10.1016/j.jhazmat.2007.08.024.
[37] O. Arar, E. Yavuz, U. Yuksel, N. Kabay, Separation of low concentration of fluoride from water by electrodialysis (ED) in the presence of chloride and sulfate ions, Sep. Sci. Technol. 44 (7) (2009) 1562–1573, https://doi.org/10.1080/01496390902775943.
[38] H. Strathmann, Electrodialysis, a mature technology with a multitude of new applications, Desalination 264 (3) (2010) 268–288, https://doi.org/10.1016/j.desal.2010.04.069.
[39] W.J. Koros, Y.H. Ma, T. Shimidzu, Terminology for membranes and membrane processes (IUPAC recommendations 1996), Pure Appl. Chem. 68 (7) (1996) 1479–1489, https://doi.org/10.1351/pac199668071479.
[40] Y. Kim, W.S. Walker, D.F. Lawler, Electrodialysis with spacers: effects of variation and correlation of boundary layer thickness, Desalination 274 (1-3) (2011) 54–63, https://doi.org/10.1016/j.desal.2011.01.076.
[41] A. Campione, L. Gurreri, M. Ciofalo, G. Micale, A. Tamburini, A. Cipollina, Electrodialysis for water desalination: a critical assessment of recent developments on process fundamentals, models and applications, Desalination 434 (2018) 121–160, https://doi.org/10.1016/j.desal.2017.12.044.
[42] I. Stenina, D. Golubenko, V. Nikonenko, A. Yaroslavtsev, Selectivity of transport processes in ion-exchange membranes: relationship with the structure and methods for its improvement, Int. J. Mol. Sci. 21 (15) (2020) 5517, https://doi.org/10.3390/ijms21155517.
[43] D. Pletcher, R. Greff, R. Peat, L. Peter, J. Robinson, Instrumental methods in electrochemistry, Elsevier, 2001. http://eprints.soton.ac.uk/id/eprint/344874.
[44] M. La Cerva, L. Gurreri, M. Tedesco, A. Cipollina, M. Ciofalo, A. Tamburini, G. Micale, Determination of limiting current density and current efficiency in electrodialysis units, Desalination 445 (2018) 138–148, https://doi.org/10.1016/j.desal.2018.07.028.
[45] V.V. Nikonenko, A.V. Kovalenko, M.K. Urtenov, N.D. Pismenskaya, J. Han, P. Sistat, G. Pourcelly, Desalination at overlimiting currents: state-of-the-art and perspectives, Desalination 342 (2014) 85–106, https://doi.org/10.1016/j.desal.2014.01.008.
[46] T. Bellon̆, Z. Slouka, Overlimiting convection at a heterogeneous cation-exchange membrane studied by particle image velocimetry, J. Membr. Sci. 643 (2022), 120048, https://doi.org/10.1016/j.memsci.2021.120048.
[47] M. Isaacson, A.A. Sonin, Sherwood number and friction factor correlations for electrodialysis systems, with application to process optimization, Ind. Eng. Chem. Process. Des. Dev. 15 (2) (1976) 313–321, https://doi.org/10.1021/i260058a017.
[48] D.A. Cowan, J.H. Brown, Effect of turbulence on limiting current in electrodialysis cells, Ind. Eng. Chem. 51 (12) (1959) 1445–1448, https://doi.org/10.1021/ie50600a026.
[49] L. Karimi, A. Ghassemi, An empirical/theoretical model with dimensionless numbers to predict the performance of electrodialysis systems on the basis of operating conditions, Water Res. 98 (2016) 270–279, https://doi.org/10.1016/j.watres.2016.04.014.
[50] O.S. Burheim, F. Seland, J.G. Pharoah, S. Kjelstrup, Improved electrode systems for reverse electro-dialysis and electro-dialysis, Desalination 285 (2012) 147–152, https://doi.org/10.1016/j.desal.2011.09.048.
[51] S.B. Solberg, P. Zimmermann, Ø. Wilhelmsen, J.J. Lamb, R. Bock, O.S. Burheim, Heat to hydrogen by reverse electrodialysis—using a non-equilibrium thermodynamics model to evaluate hydrogen production concepts utilising waste heat, Energies 15 (16) (2022) 6011, https://doi.org/10.3390/en15166011.
[52] O.S. Burheim, Engineering Energy Storage, Academic press, 2017.
[53] E. Fontananova, D. Messana, R. Tufa, I. Nicotera, V. Kosma, E. Curcio, W. Van Baak, E. Drioli, G. Di Profio, Effect of solution concentration and composition on the electrochemical properties of ion exchange membranes for energy conversion, J. Power Sources 340 (2017) 282–293, https://doi.org/10.1016/j.jpowsour.2016.11.075.
[54] K. Kontturi, L. Murtomäki, J.A. Manzanares, Ionic Transport Processes in Electrochemistry and Membrane Science, Oxford University Press Inc, 2008, https://doi.org/10.1093/acprof:oso/9780199533817.001.0001.
[55] S. Kjelstrup, D. Bedeaux, E. Johannessen, J. Gross, Non-equilibrium Thermodynamics for Engineers, World Scientific, 2010, https://doi.org/10.1142/10286.
[56] H. Fan, N.Y. Yip, Elucidating conductivity-permselectivity tradeoffs in electrodialysis and reverse electrodialysis by structure-property analysis of ion-exchange membranes, J. Membr. Sci. 573 (2019) 668–681, https://doi.org/10.1016/j.memsci.2018.11.045.
[57] R. Kingsbury, O. Coronell, Modeling and validation of concentration dependence of ion exchange membrane permselectivity: significance of convection and Manning's counterion condensation theory, J. Membr. Sci. 620 (2021), 118411, https://doi.org/10.1016/j.memsci.2020.118411.
[58] S. Ozkul, J.J. van Daal, N.J. Kuipers, R.J. Bisselink, H. Bruning, J.E. Dykstra, H. H. Rijnaarts, Transport mechanisms in electrodialysis: the effect on selective ion transport in multi-ionic solutions, J. Membr. Sci. 665 (2023), 121114, https://doi.org/10.1016/j.memsci.2022.121114.
[59] S. Abdu, M.-C. Martí-Calatayud, J.E. Wong, M. García-Gabaldón, M. Wessling, Layer-by-layer modification of cation exchange membranes controls ion selectivity and water splitting, ACS Appl. Mater. Interfaces 6 (3) (2014) 1843–1854, https://doi.org/10.1021/am4048317.
[60] L. Wang, C. Violet, R.M. DuChanois, M. Elimelech, Derivation of the theoretical minimum energy of separation of desalination processes, J. Chem. Educ. 97 (12) (2020) 4361–4369, https://doi.org/10.1021/acs.jchemed.0c01194.
[61] P. Atkins, Atkins' Physical Chemistry. Eng, Eleventh edition, Oxford University Press, Oxford, 2018.
[62] K.S. Pitzer, G. Mayorga, Thermodynamics of electrolytes. II. Activity and osmotic coefficients for strong electrolytes with one or both ions univalent, J. Phys. Chem. 77 (19) (1973) 2300–2308, https://doi.org/10.1021/j100638a009.
[63] M.C. Simoes, K.J. Hughes, D.B. Ingham, L. Ma, M. Pourkashanian, Estimation of the pitzer parameters for 1–1, 2–1, 3–1, 4–1, and 2–2 single electrolytes at 25° C, J. Chem. Eng. Data 61 (7) (2016) 2536–2554, https://doi.org/10.1021/acs.jced.6b00236.
[64] C.B. Smith, K.E. Parmenter, Chapter 7 - energy analysis, in: C.B. Smith, K. E. Parmenter (Eds.), Energy Management Principles, Second Edition, Elsevier, Oxford, 2016, pp. 95–123, https://doi.org/10.1016/B978-0-12-802506-2.00007-0.
[65] Y. Zhao, K. Tang, Q. Liu, B.Van der Bruggen, A.S. Diaz, J. Pan, C. Gao, J. Shen, Recovery of chemically degraded polyethyleneimine by a re-modification method: prolonging the lifetime of cation exchange membranes, RSC Adv. 6 (20) (2016) 16548–16554, https://doi.org/10.1039/C5RA27916J.